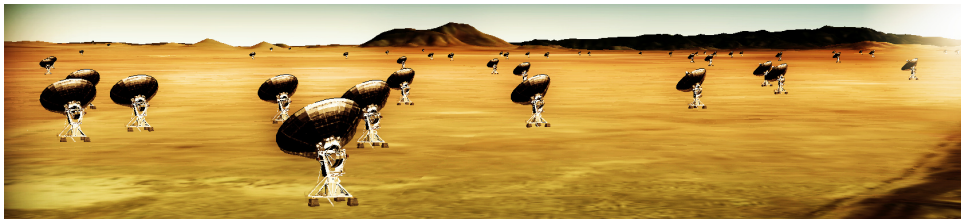

Next Generation Very Large Array Memo No. 35

Deep Fields at 8GHz

C.L. Carilli, G.C. Jones (NRAO, PO Box O, Socorro, NM), P. Sims (Brown Univ.)

Abstract

We investigate the ability of the ngVLA reference configuration to perform deep field imaging at 8GHz, in the context of galaxy formation. We adopt the ngVLA reference design configuration, but use only the antennas on the Plains of San Augustin ($\sim$ 30km max baselines). We employ a sky model generated for a $6'$ FoV, using the S-cubed sky simulation tool. We investigate Briggs weighting, and find that a value of $R \sim 0$ provides a reasonable PSF and noise performance, with a FWHM of $0.36''$ (vs. the UN weighting PSF of $0.25''$), and an rms of 65 nJy beam^{-1} (vs. the theoretical thermal noise of 50 nJy beam^{-1}). For a point-source only model, sources stronger than 10σ are well recovered, with upper limits to sizes less than the PSF. Sources at the $\sim 5\sigma$ level are reliably detected, but noise can make the point sources appear either more extended, or smaller than, the synthesized beam. For a model in which all the sources are Gaussian with a size of $\sim 1.2''$, the bright sources ($> 10\sigma$ peak surface brightness), are well recovered in terms of size, peak surface brightness, and total flux density. Fainter sources appear significantly larger than their true sizes, with a higher total flux density. The over-extended faint sources arise from incomplete cleaning of wings of the synthesized beam. We also find that the Gaussian sources look 'mottled', along the lines of the classic CLEAN instability. Multiscale clean does not fix this problem (nor does a lower loop gain). For a mixed model of mostly point sources, plus a few extended sources, the extended sources can be recovered more accurately, since CLEAN does not have to work as hard.

1 Introduction

Radio deed fields are an important tool in studies of galaxy formation. Radio deep fields reveal distant star forming galaxies, AGN, and clusters. High

resolution imaging can be used to determine source sizes (Cotton et al. 2018).

The ngVLA will be a powerful tool to perform radio deep fields, reaching nano-Jy sensitivity. However, the non-reconfigurable, tri-scale array presents a challenge to obtain both a reasonable synthesized beam and good sensitivity (Carilli 2016; 2017). Cotton & Condon (2017), have recently considered deep fields at 3GHz for the ngVLA, tapered to $0.5''$ resolution. In their work, they emphasize high dynamic range imaging ($\sim 10^5$), and they explore three different array configurations.

Herein, we perform simulations at 8GHz. We consider just the reference array design, and investigate imaging parameters to optimize the PSF and the sensitivity. We consider the reference array's ability to recover faint point sources, and faint extended sources.

2 Simulated Sky

We employ the Southwest configuration of the reference design of the ngVLA (Carilli 2017, 2016; Selina & Murphy 2017). The array has 214 total number of antennas, with about 40% of the antennas in a dense core of diameter ~ 1.5km (the Core), another 40% of the antennas to 30km (the Plains), and the rest to distances of a few hundred km (the Spiral).

The cosmological sources of interest are galaxies. These are typically small, but extended on scales $\sim 0.1''$ to $1''$. Hence, we target a resolution of $\sim 0.3''$, and we include only the Core and Plains antennas (168 antennas).

We observe at 8 GHz. We do not perform a multifrequency synthesis (see Discussion section), but we calculate the noise based on a 4GHz bandwidth. We perform a 4hour synthesis, and assume 10 days of observation, for 40hrs total. We use system parameters from Selina & Murphy (2017), with $T_{sys} =$ 22K, an 18m antenna diameter, $\epsilon = 75\%$ efficiency, dual polarization, and N = 168 antennas. The implied theoretical sensitivity (ideal weighting, no confusion or sidelobe noise), is:

$$\mathrm{rms} = 1.03 \times \frac{\mathrm{T_{sys}}}{\epsilon \mathrm{A_{m^2}}} \times (\Delta\nu_{\mathrm{kHz}} \times \mathrm{t_{hr}} \times \mathrm{N(N-1)})^{-0.5} \sim 50 \ \mathrm{nJy\ beam^{-1}}$$

We employ the CASA simulator for the ngVLA, described in (Carilli et al. 2017).

Our model sky was generated using the S-cubed radio sky simulations developed for the SKA project (Wilman et al. 2008). We simulate a $6'$ field

of view, with $0.05''$ pixels. The model includes 6000 sources in a powerlaw distribution in number density, ranging from 100nJy to 1mJy.

We create three models. First is a point source-only model, with the peak = total flux densities in the range listed above. The second involves all Gaussian sources, with sizes of FWHM = $1.2''$, and total flux densities as per the distribution above. In this case, the peak surface brightness are then correspondingly lower. Third, we then added a few Gaussians of different sizes to the all-point source model.

3 Robust Comparisons

Figure 1 shows the image of the full field from the all-Gaussian model, made with CLEAN and Briggs weighting with Robust, $R = 0$. This image was made using a multi-scale clean.

Figure 2 shows blow-up images with $R = -0.7$ (approaching Uniform weighting), $R = 0$, and $R = +0.7$ (approaching Natural weighting). The corresponding synthesized beams are shown in Figure 3, along with 1D horizontal cuts through the beam. The key issue is clear in the beam cut image: as the weighting approaches Natural, the dense core generates broad wings out to a $\sim 2''$, at the $\sim 20\%$ level. These wings are problematic for high fidelity imaging (Carilli 2016; Cotton & Condon 2017).

We then explored imaging with R varying continuously from -2.0 to +2.0, in increments of 0.1. The resulting restoring beams and RMS noise levels are reported in Table 1, and are plotted in Figure 4. We use 8000 clean iterations, and the all-point source model.

The FWHM of the restoring beam increases slowly between $R = -2.0$ and 0.4, increases steeply between 0.5 and 1.4, and flattens out again between 1.4 and 2.0. From natural to uniform weighting, the beam FWHM varies by a factor of ~ 17.

The RMS noise level shows a low constant value of $\sim$ 100nJy beam^{-1} between $R = -2.0$ and -1.2, a dip to a broad minimum of $\sim$ 65nJy beam^{-1} for $R \sim -0.3$ to +0.5. Then a sharp rise to $\sim$ 240nJy beam^{-1} at $R > +1$. Again, the ideal theoretical noise for this observation would be $\sim$ 50nJy beam^{-1}. The increase in the noise at low values of R is due to the down-weighting of all the antennas in the Core. The increase in the noise at the high values of R occurs due 'sidelobe confusion', due to the residual, uncleaned, very broad wings of the synthesized beam from all the faint sources.

Overall, the range around $R \sim 0$ provides sufficient resolution for the

science ($\sim 0.36''$), and a noise value that is close to optimal for this tri-scale array, with a loss of about 40% in sensitivity compared to the theoretical thermal noise for the Plains array. The PSF still shows a non-Gaussian wing, but less much pronounced than for larger R values, dropping below 10% at about $0.4''$ radius (for a Gaussian, the value would be 3.3% at this radius). Such a beam has been shown to perform adequately in a number of the Key Science programs (Ricci et al. 2018; Carilli & Shao 2017), and we adopt R = 0 as nominal for the imaging tests below.

4 Recovering Point Sources

We next consider the recovery of point sources in a deep image, using the all-point source model. In this case, we use $R = 0$, and CLEAN to 40000 iterations, reaching a minimum CLEAN component of $\sim 2.3\sigma$ (140 nJy). The rms on the final image is 65 nJy beam^{-1}.

Figure 5 shows a blow up of a region in the image, with a few sources numbered for reference. We have fit Gaussians to these sources, to investigate the apparent sizes and flux densities of the sources after imaging. The results are listed in Table 2. For the bright sources ($\sim 10\sigma$), the source flux densities and sizes are well recovered, with size limits less than the synthesized beam size, and flux densities as expected from the input model.

For the two fainter sources investigated, ~ 4 to 5σ, the flux densities from the fitting can be significantly different than the model, as well as the sizes. In one case (P8), the model fit suggests a much larger, and stronger, source than the model. The reverse is true for P7. These results represent the combined effect of noise, imaging, and possibly confusion, on recovering fainter point sources in the field: the sources are well detected, but their parameterization via Gaussian fitting can be errant.

5 Recovering Extended sources: All Gaussian Model

The next extreme we consider is an all-Gaussian model, in which all the sources are extended with a FWHM of $1.2''$. The source total flux density distribution is the same as the all-point source model, but the emission is distributed over the Gaussian sizes, leading to lower peak surface brightnesses. In this case, CLEAN will have to work harder to clean out the wings of fainter sources.

We investigate three different CLEAN options: a shallower CLEAN with 8000 iterations, reaching a minimum clean component of 320 nJy, a

deeper clean to 40000 iterations, and reaching a minimum clean component of 140nJy, and a deep multi-scale clean to 40000 iterations. In all cases, we reach an rms on the final image of about 65 nJy beam^{-1}.

Figure 6 shows a blow up of the same region as Figure 5, but now for the all-Gaussian source model. A few sources are labeled, and the results for fitting Gaussian models to these sources are given in Table 3[1]. For the brightest source in the sub-image (peak surface brightness $\sim 100\sigma$), the fit source size, peak, and total flux density are in good agreement with the input model. For the fainter sources, the fits get worse with decreasing flux density, as the peak surface brightness drops below 10σ. The sizes are over-estimated substantially, as are the total flux densities. The solutions get better with the deeper CLEAN, but are still not accurate relative to the expected model. This over-estimate is likely, again, due to residual uncleaned wings of the PSF perturbing the solutions in a Gaussian fitting process in which the intrinsic PSF is assumed to be Gaussian in shape.

Perhaps more importantly, the sources themselves looked 'mottled' in appearance – sub-peaks and clumps across what should be a Gaussian profile. This appearance is reminiscent of the standard CLEAN instability for extended sources, as the CLEAN algorithm attempts to decompose diffuse sources into point-source components (Cornwell 1983).

To address the mottled appearance of the sources, we attempted a deep multi-scale CLEAN. This process was much slower than the standard CLEAN, and the results are identical, as shown in Figure 6.

6 Recovering Extended Sources: Few Gaussian Model

As a final, intermediate case, we insert Gaussian sources of different sizes and flux densities, into the point-source only model. In this case, CLEAN may not have to work as hard to deconvolve the sources and recover the source parameters. A deep clean was again employed, to $\sim$ 100 nJy minimum CLEAN component.

The Gaussian fit results are summarized in Table 4. The sources range from $0.25''$ to $1''$ in size, and total flux densities of 1μJy and 5μJy. The peak surface brightnesses extend down to 2.5σ.

The bright and small sources are clearly recovered nicely, both in terms of intrinsic size and total flux density. The fainter source fits are larger than

[1]SSC = Shallow (8000 iteration), single-scale CLEAN. DSSC = Deep (40000 iteration), single-scale CLEAN.

the intrinsic models, and the total flux densities are higher than the input models, as in section 5.

As an additional test case, we ran TCLEAN on the above data set, using only 6000 CLEAN iterations. This resulted in poor results for the 1 μJy sources. The recovered sizes were $2-3\times$ larger than the original scales, as were the flux densities. In this case, the faintest, largest source is essentially undetected in the final image.

7 Discussion

We have simulated deep field observations with the reference configuration of the ngVLA at 8GHz, using the Plains configuration out to 30km maximum baseline. We employ a sky model generated for a 6arcmin FoV, using the S-cubed sky simulation tool. We investigate a point-source only model, a Gaussian-source only model, and a mixed model. The main results are as follows:

- We find that a value of $R \sim 0$ provides a reasonable PSF and noise performance, with a FWHM of $0.36''$ (vs. the UN weighting PSF of $0.25''$), and an rms of 65 nJy beam^{-1} (vs. the theoretical thermal noise of 50 nJy beam^{-1}).

- All point source model: sources stronger than 10σ are well recovered. For sources at the $\sim 5\sigma$ level, noise, confusion, and other effects can make the point sources appear either extended, or smaller than the synthesized beam.

- All Gaussian source model: the bright sources ($> 10\sigma$ peak surface brightness), are well recovered. Fainter sources appear significantly larger than their true sizes, with a higher total flux density. This over-extension likely arises from incomplete cleaning of wings of the synthesized beam. The sources look 'mottled', along the lines of the classic CLEAN instability for extended sources. Multiscale clean does not fix this problem.

- Few Gaussian source model: the extended sources can be recovered more accurately, since CLEAN does not have to work as hard. However, faint, large sources remain difficult to recover.

While we have assumed the sensitivity of a 4GHz system, we have not included a full bandwidth synthesis for the uv-coverage. Bandwidth synthesis will certainly fill-in the uv-plane. However, we do not believe bandwidth

synthesis will solve the CLEAN instability problem, which may be the most problematic of the issues encountered.

We emphasize that this study is only representative, not exhaustive. For instance, the non-Gaussian wing of the PSF for our nominal R = 0 weighting suggests that perhaps determining source sizes and flux densities via Gaussian fitting and parameterization is not the most accurate approach. Required Future work includes a broader investigate of weighting (Briggs, tapers, and cell size), and alternative configurations on Plains-scales. Further algorithmic development is also clearly required for deep deconvolution of fuzzy sources.

8 Addendum

As another test on deep CLEAN and extended sources, we reimaged the field using the all-Gaussian field with the same parameters as in the Figure 6 for the multi-scale clean, but now with a lower loop gain (0.03 now, vs. 0.1 in figure 6), and more clean iterations (120,000). The idea is that a lower loop gain may solve the mottled source problem. In this case, the processing takes a factor few longer than previously. With 120,00 iterations, we reach a minimum CLEAN component of 0.21nJy ($\sim 3\sigma$).

The resulting image is shown in Figure 7. The results are essentially unchanged: the fainter Gaussian sources have a very similar mottled appearance as compared to the image made with a higher loop gain.

References

Carilli, C. 2016, ngVLA memo 12
Carilli, C. 2017, ngVLA memo 16
Carilli & Shao 2017, ngVLA memo 13
Carilli, Greisen, Nyland, Indebetouw 2017, ngVLA CASA simulator Guide
Cornwell, T. 1983, A& A, 121, 281
Cotton & Condon 2017, ngVLA memo 30
Cotton, B. et al. 2018, ApJ, in press (arXiv:1802.04209)
Ricci et al. 2018, ngVLA memo 33
Selina & Murphy 2017, ngVLA memo 17
Wilman et al. 2008, MNRAS, 388, 1335

Table 1: Beam sizes and noise levels vs. Robust parameter

Robust	Restoring beam arcsec, PA(deg)	RMS nJy beam^{-1}	Robust	Restoring beam arcsec, PA(deg)	RMS nJy beam^{-1}
2.0	4.85×4.48 , 45.16	242	-0.1	0.35×0.34 , -4.22	69
1.9	4.85×4.47 , 45.17	242	-0.2	0.33×0.32 , -3.28	70
1.8	4.84×4.47 , 45.18	241	-0.3	0.32×0.31 , -2.8	73
1.7	4.83×4.46 , 45.19	241	-0.4	0.31×0.30 , -2.89	76
1.6	4.82×4.45 , 45.22	240	-0.5	0.30×0.29 , -3.08	79
1.5	4.69×4.33 , 44.65	235	-0.6	0.29×0.28 , -1.91	82
1.4	4.66×4.27 , 61.98	230	-0.7	0.28×0.27 , -2.53	86
1.3	4.60×4.06 , 67.43	222	-0.8	0.28×0.26 , -2.54	90
1.2	4.37×3.85 , 68.00	221	-0.9	0.27×0.26 , -2.41	94
1.1	4.10×3.62 , 68.49	208	-1.0	0.27×0.26 , -2.50	97
1.0	3.71×3.26 , 69.26	196	-1.1	0.26×0.25 , -2.59	99
0.9	2.92×2.54 , 36.17	157	-1.2	0.26×0.25 , -2.68	101
0.8	1.15×1.03 , 21.48	105	-1.3	0.26×0.25 , -2.71	102
0.7	0.88×0.78 , 39.36	83	-1.4	0.26×0.25 , -3.73	103
0.6	0.77×0.69 , 22.26	74	-1.5	0.26×0.25 , -3.75	103
0.5	0.62×0.59 , 45.23	69	-1.6	0.26×0.25 , -3.76	104
0.4	0.49×0.45 , -24.82	65	-1.7	0.26×0.25 , -3.77	104
0.3	0.44×0.42 , -0.24	64	-1.8	0.26×0.25 , -3.78	104
0.2	0.41×0.40 , -1.85	64	-1.9	0.26×0.25 , -3.78	104
0.1	0.38×0.37 , -3.47	66	-2.0	0.26×0.25 , -3.78	104
0.0	0.37×0.36 , -3.13	67			

Table 2: Recovering Point Sources

Source	Image	FWHM arcsec	S_ν μJy	Peak I_ν μJy beam^{-1}
P5 3652, 2880	Model	0	0.61	0.61
P5 3652, 2880	DSSC	$\leq 0.32 \times 0.14$	0.65 ± 0.1	0.56 ± 0.06
P6 3786, 2998	Model	0	0.55	0.55
P6 3786, 2998	DSSC	$\leq 0.24 \times 0.11$	0.64 ± 0.1	0.62 ± 0.06
P7 3630, 3041	Model	0	0.39	0.39
P7 3630, 3041	DSSC	Fit size $<$ Syn Beam	0.28 ± 0.1	0.34 ± 0.06
P8 3607, 2998	Model	0	0.34	0.34
P8 3607, 2998	DSSC	$1.1 \times 0.44 \pm 0.43$	1.0 ± 0.34	0.21 ± 0.064

Table 3: Recovering Extended Sources: All Gaussian Model

Source	Image	FWHM arcsec	S_ν μJy	Peak I_ν μJy beam^{-1}
G1 3488, 2917	Model	1.2	89	8.3
G1 3488, 2917	SSC	$1.25 \times 1.24 \pm 0.15$	97 ± 1	7.6 ± 0.08
G1 3488, 2917	DSSC	$1.21 \times 1.21 \pm 0.12$	93 ± 1	7.6 ± 0.08
G2 3641, 3121	Model	1.2	6.8	0.59
G2 3641, 3121	SSC	$1.71 \times 1.60 \pm 0.1$	15.4 ± 0.9	0.71 ± 0.04
G2 3641, 3121	DSSC	$1.52 \times 1.41 \pm 0.1$	11.2 ± 0.7	0.64 ± 0.04
G3 4067, 3056	Model	1.2	3.9	0.36
G3 4067, 3056	SSC	$2.1 \times 1.7 \pm 0.15$	12.2 ± 0.6	0.43 ± 0.03
G3 4067, 3056	DSSC	$2.0 \times 1.5 \pm 0.20$	8.2 ± 0.8	0.34 ± 0.03
G4 3535, 2773	Model	1.2	2.5	0.24
G4 3535, 2773	SSC	$1.8 \times 1.7 \pm 0.2$	7.8 ± 0.9	0.33 ± 0.035
G4 3535, 2773	DSSC	$1.7 \times 1.4 \pm 0.25$	5.2 ± 0.8	0.27 ± 0.03

Table 4: Recovering Extended Sources: Few Gaussian Model

FWHM arcsec	Model S_ν μJy	FWHM arcsec	S_ν μJy	Peak I_ν μJy beam^{-1}
0.25	1.0	$0.37 \times 0.21 \pm 0.08$	1.3 ± 0.2	0.77 ± 0.06
0.25	5.0	$0.27 \times 0.26 \pm 0.02$	5.1 ± 0.2	3.34 ± 0.06
0.50	1.0	$0.6 \times 0.5 \pm 0.1$	1.2 ± 0.2	0.39 ± 0.06
0.50	5.0	$0.56 \times 0.52 \pm 0.03$	5.3 ± 0.3	1.64 ± 0.06
1.00	1.0	$1.8 \times 1.1 \pm 0.3$	2.4 ± 0.6	0.15 ± 0.04
1.00	5.0	$1.2 \times 1.1 \pm 0.1$	6.8 ± 0.5	0.61 ± 0.05

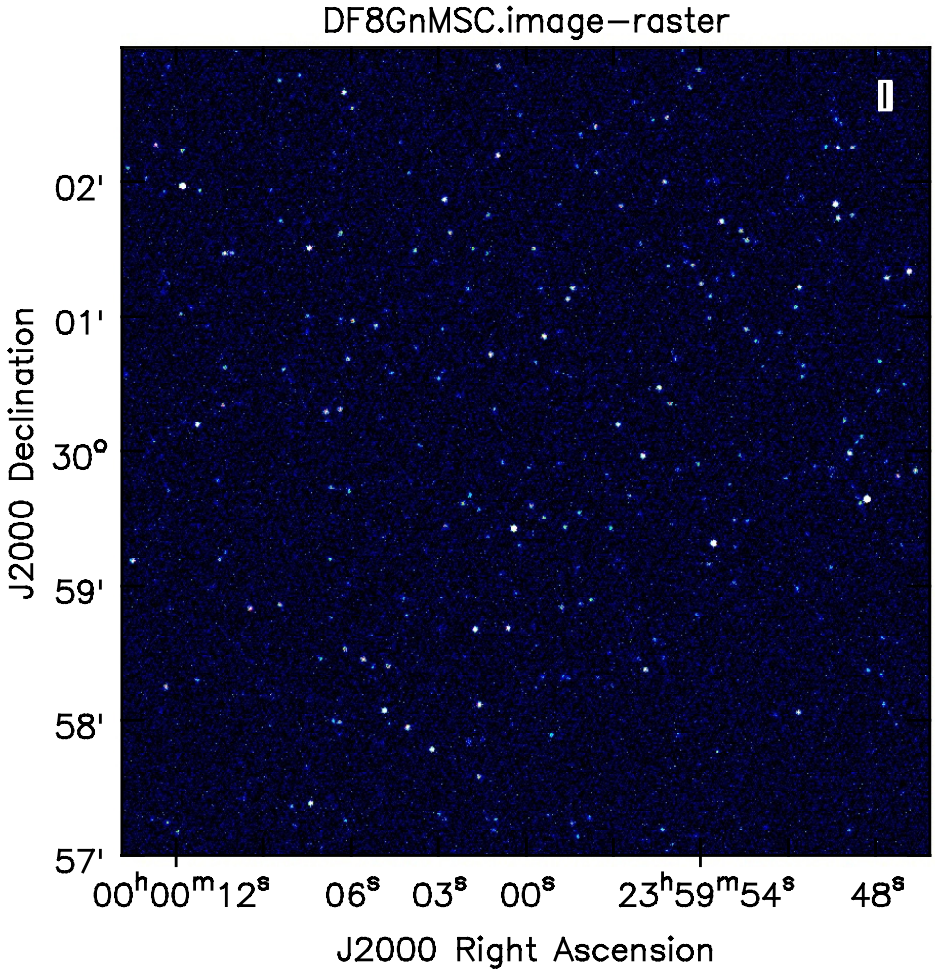

Figure 1: The full field for the Gaussian model image of the S-Cubed simulation at 8GHz for the ngVLA with Robust = 0, assuming 10 x 4 hours of observation. There are a total of 6000 sources in the field, ranging from 100nJy to 1mJy total flux density. The noise level is 65 nJy beam^{-1}, and the synthesized beam FWHM = 0.36″.

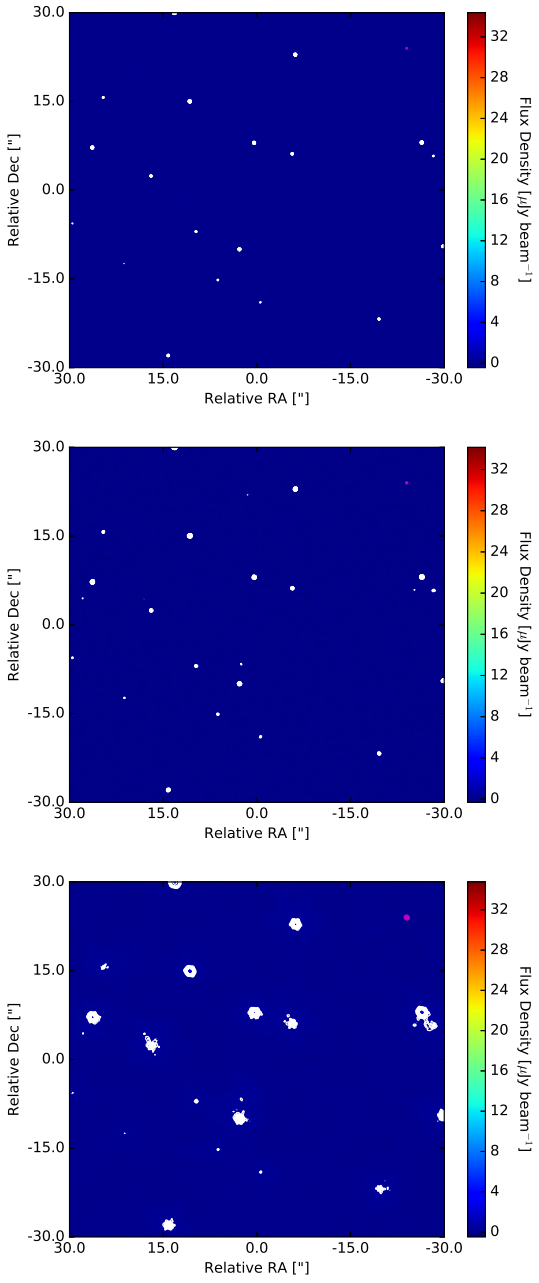

Figure 2: An example field from our simulation, imaged using robust=-0.7 (top), 0.0 (center), and 0.7 (bottom). Contours are shown at $\pm 5, 6, 7, ... \sigma$, and the restoring beams are shown in the upper right corners of each.

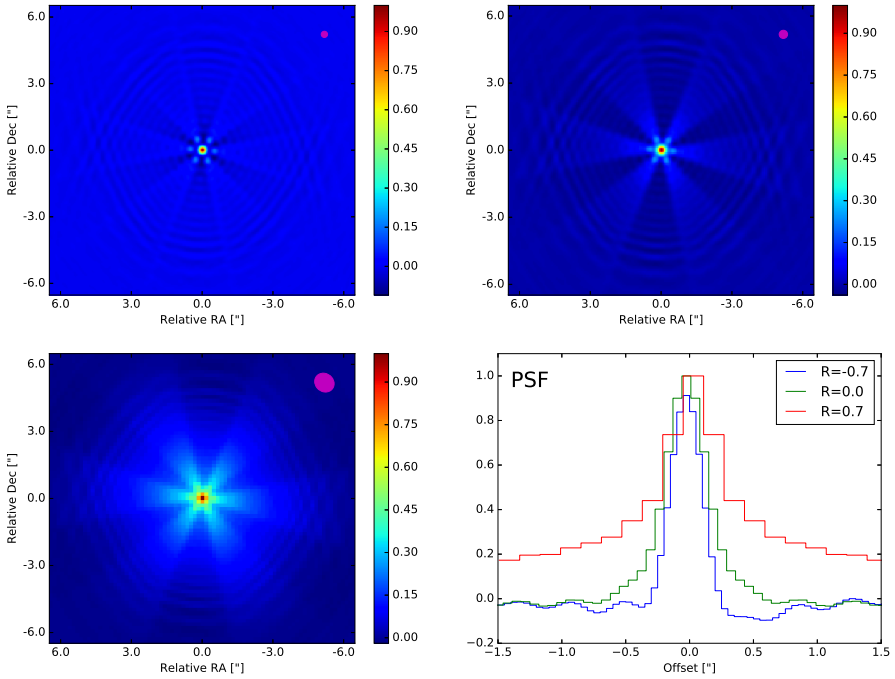

Figure 3: Results of robust=-0.7, 0.0, and 0.7, starting at the top. Bottom: Horizontal slices across the center of the PSF. Notice the large plateau extending to $> 1.5''$ at the 20% level for weighting that approaches Natural. This broad arises from the dense core of the array.

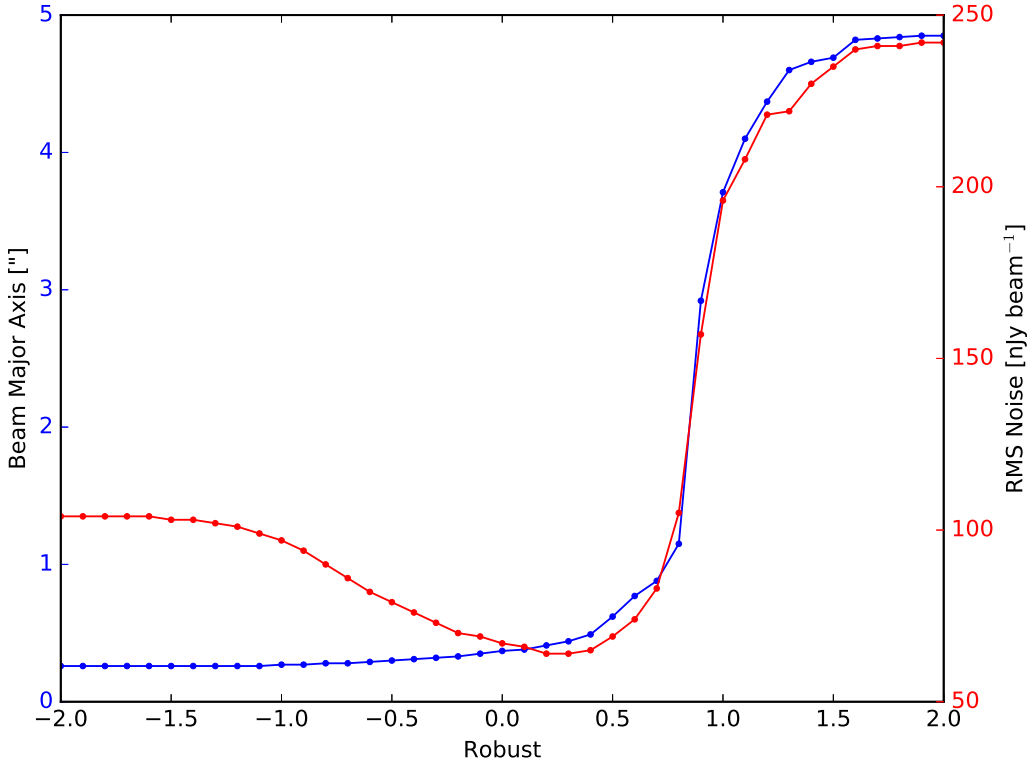

Figure 4: The FWHM of the restoring beam (blue) and the RMS noise level (red) for each robust value.

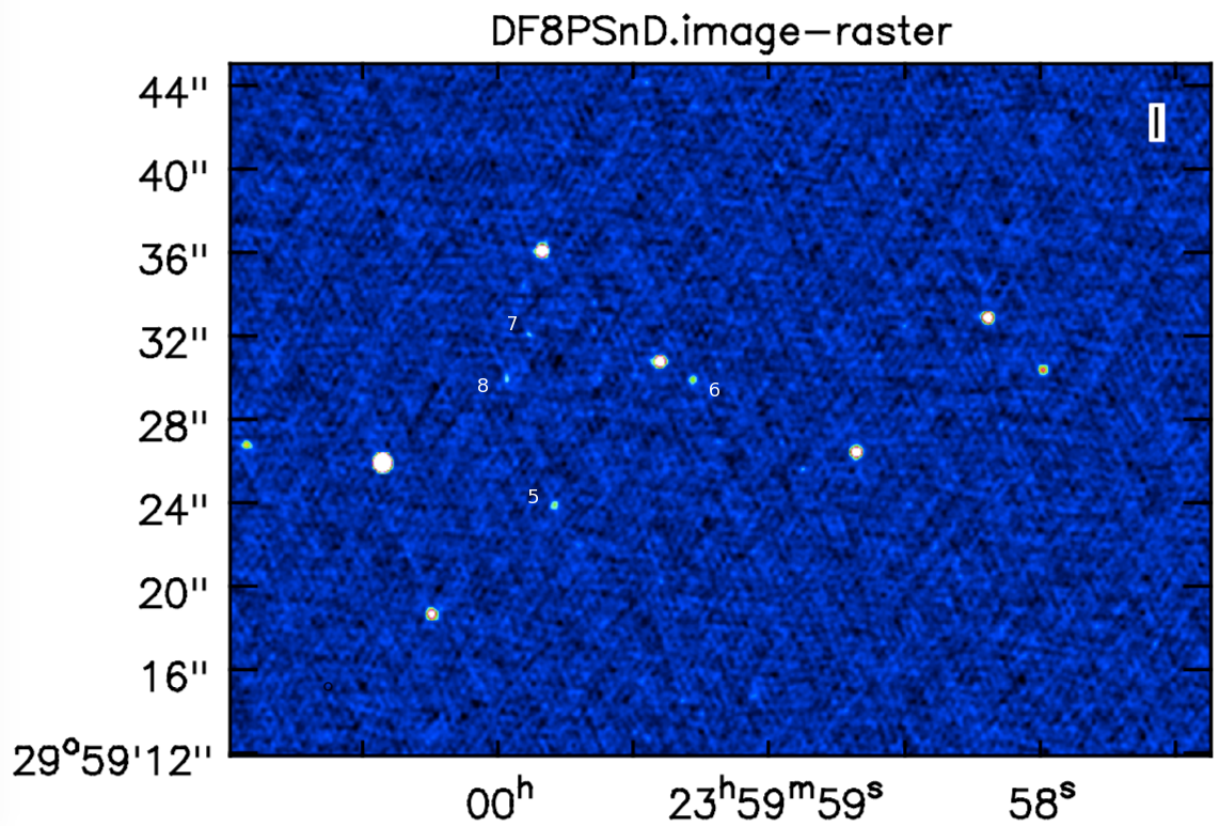

Figure 5: Blow-up of a region in the point source model image for the ngVLA with Robust = 0, assuming 10 x 4 hours of observation. The noise level is 65 nJy beam^{-1}, and the synthesized beam FWHM = 0.36″.

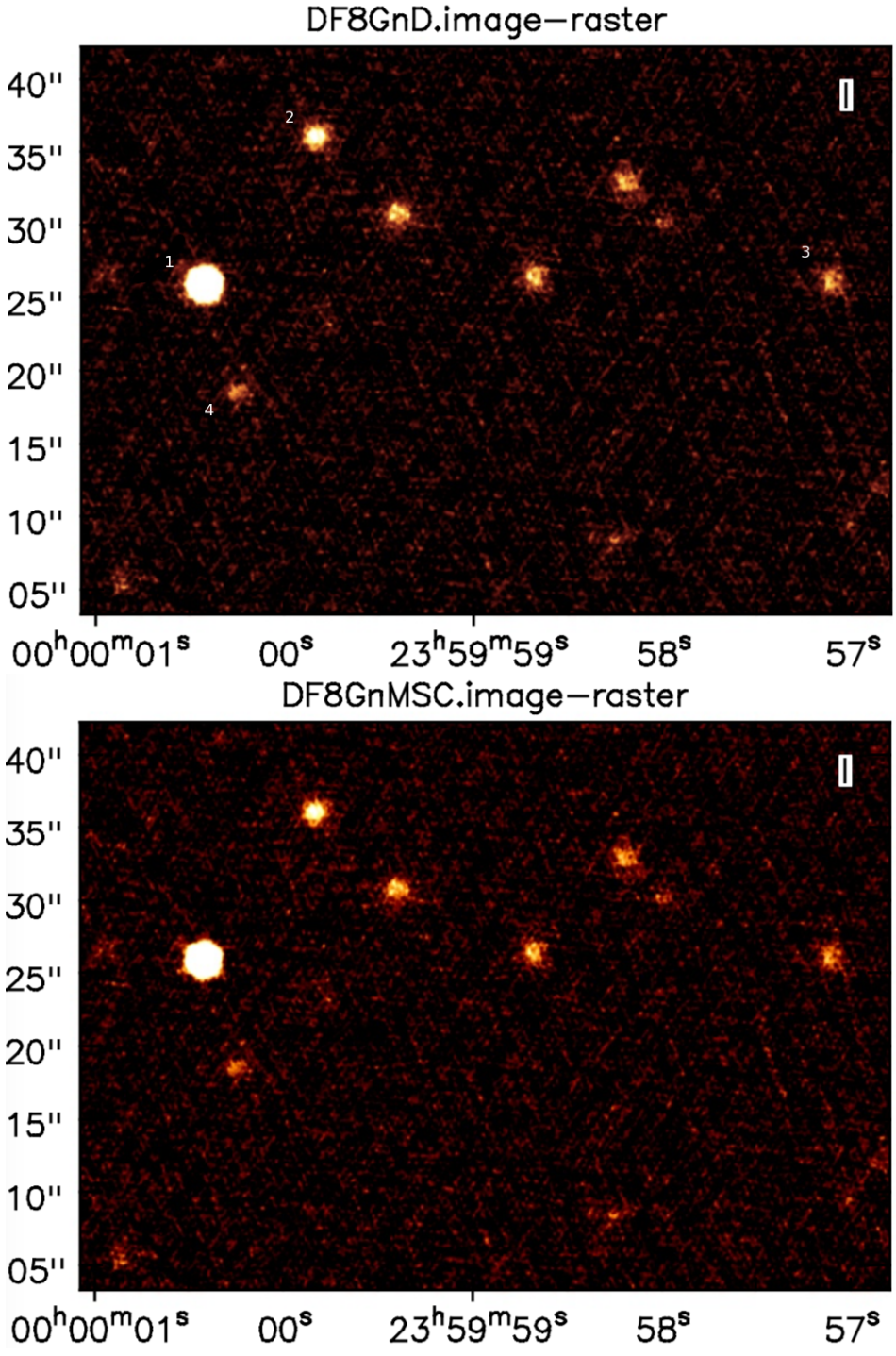

Figure 6: Blow-up of a region in the Gaussian source model image for the ngVLA with Robust = 0, assuming 10 x 4 hours of observation. The noise level is 65 nJy beam^{-1}, and the synthesized beam FWHM = 0.36″. Top: Multi-scale CLEAN was not applied. Bottm: With Multi-scale CLEAN.

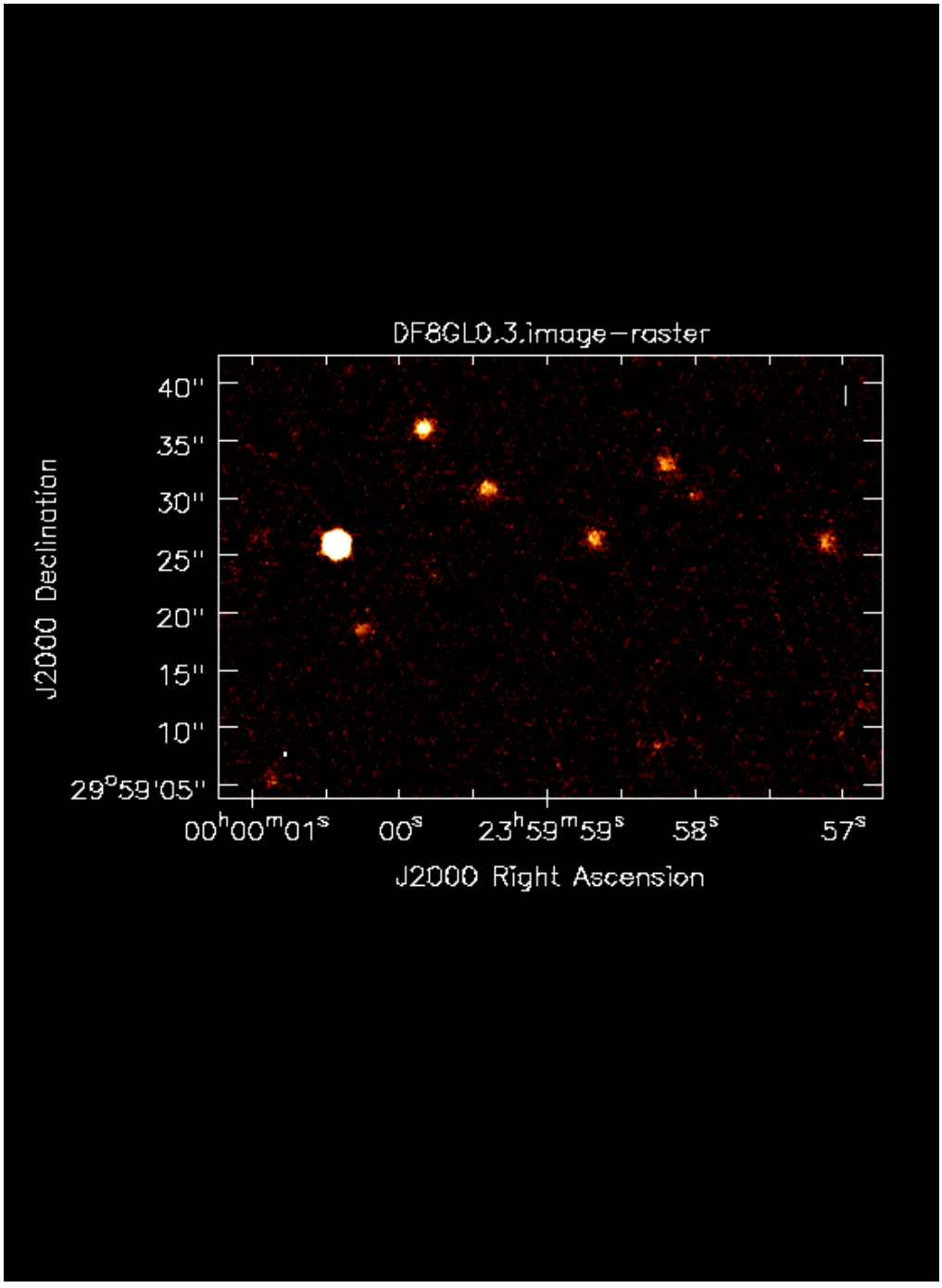

Figure 7: Same as figure 6, but now using a deep multi-scale CLEAN, and a CLEAN loop gain of 0.03 instead of 0.1. A total of 120,000 clean iterations were employed.